

On the Sample Efficiency of Inverse Dynamics Models for Semi-Supervised Imitation Learning

Sacha Morin^{1,2*} Moonsub Byeon³ Alexia Jolicoeur-Martineau⁴ Sébastien Lachapelle⁴

Abstract

Semi-supervised imitation learning (SSIL) consists in learning a policy from a small dataset of action-labeled trajectories and a much larger dataset of action-free trajectories. Some SSIL methods learn an inverse dynamics model (IDM) to predict the action from the current state and the next state. An IDM can act as a policy when paired with a video model (VM-IDM) or as a label generator to perform behavior cloning on action-free data (IDM labeling). In this work, we first show that VM-IDM and IDM labeling learn the same policy in a limit case, which we call the IDM-based policy. We then argue that the previously observed advantage of IDM-based policies over behavior cloning is due to the superior sample efficiency of IDM learning, which we attribute to two causes: (i) the ground-truth IDM tends to be contained in a lower complexity hypothesis class relative to the expert policy, and (ii) the ground-truth IDM is often less stochastic than the expert policy. We argue these claims based on insights from statistical learning theory and novel experiments, including a study of IDM-based policies using recent architectures for unified video-action prediction (UVA). Motivated by these insights, we finally propose an improved version of the existing LAPO algorithm for latent action policy learning. We experiment on the ProcGen, Push-T and Libero benchmarks.

1. Introduction

Behavior cloning (BC) (Pomerleau, 1988) is a capable technique for learning control policies via supervised learning on action-labeled expert trajectories in both state-based and

¹Département d'informatique et de recherche opérationnelle, Université de Montréal ²Mila – Quebec AI Institute ³Samsung Electronics, Suwon ⁴Samsung AI Lab, Montreal.*Work performed during an internship at Samsung AI Lab, Montreal. Correspondence to: Sacha Morin <sacha.morin@umontreal.ca>.

Preprint. February 4, 2026.

visual domains. Following the successes in natural language processing and computer vision, applying BC to large datasets is seen as a promising avenue for learning general policies in fields such as robotics (O’Neill et al., 2024). However, scaling datasets for BC requires collecting action-labeled expert demonstrations, a particularly onerous process in domains requiring human demonstrations.

There is therefore a strong interest in leveraging data that is already available “in the wild”, typically in the form of videos. Videos tend to be goal-directed and depict quasi-expert or expert behaviors that can be leveraged for policy learning. Such data, however, does not include action labels. Learning from abundant action-free data and a comparatively small dataset of action-labeled data is called *semi-supervised imitation learning* (SSIL) (Baker et al., 2022).

A number of high-performing methods for SSIL leverage an *inverse dynamics model* (IDM) to predict actions from the current and next observations. An IDM can be trained on the small, action-labeled dataset and used to synthetically label action-free data for downstream BC (IDM labeling) (Baker et al., 2022). Other methods form a policy by instead coupling the IDM with a *video model* (VM) trained on unlabeled data (VM-IDM) (Du et al., 2023). The IDM also plays an important roles in recent methods for latent action learning (Schmidt & Jiang, 2024).

To effectively leverage action-free data, IDM-based SSIL methods make the assumption that the IDM will generalize better than BC trained on the same amount of labeled data. While the sample efficiency of the IDM has been measured empirically, previous works only hypothesize partial explanations for this phenomenon, ranging from the IDM being non-causal and simpler (Baker et al., 2022) to analogies with the sample-efficiency of model-based reinforcement learning (Torabi et al., 2018).

In this work, we unify IDM-based methods and seek a more complete explanation for their success in SSIL settings. We argue that the sample efficiency of IDM learning stems from the reduced complexity and stochasticity of the ground truth IDM compared to the ground truth policy. These factors are environment-specific and offer a valuable framework for understanding when and to what extent IDM-based learning

can outperform BC. Experimentally, we explore IDM-based learning across multiple datasets and show how the statistical advantage of IDM learning can be leveraged to improve other IDM-based SSIL methods. Our key contributions are

1. We show that, at optimality, VM-IDM and IDM labeling recover the same policy when the unlabeled dataset is infinite and model capacity is sufficient. We call this common policy the IDM-based policy (Section 3).
2. We attribute the improved sample-efficiency of IDM learning over BC to two causes: (i) the ground-truth IDM tends to be contained in a lower complexity hypothesis class relative to the expert policy, and (ii) the ground-truth IDM is often less stochastic than the expert policy. We use insights from statistical learning theory and experiments to argue these claims (Section 4).
3. We present an extensive and novel comparison across the 16 ProcGen environments, Push-T and Libero, and discuss how IDM properties correlate with the increased performance of IDM-based policies over BC (Section 5).
4. Motivated by the sample-efficiency of IDM learning, we propose an improved version of the LAPO algorithm for latent action policy learning (Schmidt & Jiang, 2024) and demonstrate its superiority on the ProcGen benchmark (Section 5.1). We further show how sampling a recent architecture for unified video-action prediction (UVA) as a VM-IDM can improve policy success (Section 5.2).

2. Background & Related Work

2.1. Finite-Horizon Markov Decision Processes (MDP)

We consider a Markov decision process (MDP) with finite-horizon T , state space \mathcal{S} (e.g. positions or images), initial state distribution $p^1(s^1)$, action space \mathcal{A} , stationary transition kernel $p(s' | s, a)$ and reward function $r(s, a, s')$ (Sutton & Barto, 2018). Given a stationary policy $\pi(a | s)$, let $d_\pi(\tau)$ be the distribution over sequences $\tau := (s^1, a^1, s^2, a^2, \dots, s^T, a^T, s^{T+1})$ obtained by following policy π at each iteration. Let $p_\pi^t(s)$ be the distribution of the t th state s^t when following π . We can then define the *state visitation distribution* as $p_\pi(s) := \frac{1}{T} \sum_{t=1}^T p_\pi^t(s)$. We also define the *transition visitation distribution* as

$$p_\pi(s, a, s') := p_\pi(s)\pi(a | s)p(s' | s, a). \quad (1)$$

A sample from the above corresponds to (i) sampling a trajectory τ from d_π , (ii) sampling with uniform probability a time step $t \in \{1, \dots, T\}$, and (iii) outputting (s^t, a^t, s^{t+1}) . Let $r(\pi) := \mathbb{E}_{d_\pi(\tau)} \sum_{t=1}^T r(s^t, a^t, s^{t+1})$ be the total expected reward achieved by π .

2.2. Behavior Cloning (BC)

In BC, we are given a dataset of state-action pairs $\mathcal{D}_L := \{(s_i, a_i)\}_{i=1}^{N_L}$ sampled from p_{π^*} where π^* is an expert policy

achieving high reward. BC consists in learning a policy $\hat{\pi}$ via supervised learning on the dataset \mathcal{D}_L (Pomerleau, 1988). Given an hypothesis class Π of policies, a standard approach is to minimize the cross-entropy:

$$\hat{\pi}_{\text{BC}} \in \arg \min_{\pi \in \Pi} -\frac{1}{N_L} \sum_{i=1}^{N_L} \log \pi(a_i | s_i). \quad (2)$$

The hope is that, given enough samples, we will have that $\hat{\pi}_{\text{BC}} \approx \pi^*$ so that $r(\hat{\pi}_{\text{BC}}) \approx r(\pi^*)$.

2.3. IDM-Based Semi-Supervised Imitation Learning

The fact that expert state-action pairs are usually costly to acquire motivated the development of methods that can also leverage action-free transitions of the form (s, s') , which are typically much more abundant. In this setting, we are given a small dataset of action-labeled transitions $\mathcal{D}_L := \{(s_i, a_i, s'_i)\}_{i=1}^{N_L}$ as well as a very large dataset of unlabeled transitions $\mathcal{D}_U := \{(s_i, s'_i)\}_{i=N_L+1}^{N_L+N_U}$, assumed to have been sampled i.i.d. from $p_{\pi^*}(s, a, s')$, defined in (1). We refer to this setting as *semi-supervised imitation learning* (SSIL) (Baker et al., 2022). While our work focuses on learning offline from fixed datasets, we note a number of similar settings where \mathcal{D}_L is built online through environment interactions (Torabi et al., 2018; Radosavovic et al., 2021). The broad field of learning from action-free expert data is often discussed under the umbrella term *Learning from observations (LfO)* (Torabi et al., 2019).

We now review two methods for SSIL that rely on learning an *inverse dynamics model* (IDM) $\hat{h}(a | s, s')$ which, given a pair of consecutive states, predicts the action taken.

2.3.1. VM-IDM LEARNING

One approach to leverage this additional unlabeled dataset \mathcal{D}_U is to train a video model (VM) and combine it with an IDM to define a policy.

First, a VM $\hat{v}(s' | s)$ is trained to minimize the next state prediction loss $-\frac{1}{N} \sum_{i=1}^N \log \hat{v}(s'_i | s_i)$, where $N := N_L + N_U$, thus using all available (s_i, s'_i) . Second, an IDM $\hat{h}(a | s, s')$ is trained to predict the action a_i from the transition (s_i, s'_i) , using the small action-labeled dataset \mathcal{D}_L :

$$\hat{h} \in \arg \min_{h \in \mathcal{H}} -\frac{1}{N_L} \sum_{i=1}^{N_L} \log h(a_i | s_i, s'_i), \quad (3)$$

where \mathcal{H} is an hypothesis class of IDMs. These two models define the *VM-IDM policy* from which, given a state s , we can sample as follow: (i) sample the next-state \hat{s}' from the VM $\hat{v}(s' | s)$, and (ii) sample \hat{a} from the IDM $\hat{h}(a | s, \hat{s}')$.

A growing number of methods—particularly in robotics—can be described as VM-IDM policies. The modular nature

of VM-IDM allows to use different datasets or pretrained models for learning/defining \hat{v} and \hat{h} . For \hat{v} , a core objective is to achieve increased generalization by leveraging internet-scale action-free video data, either to train \hat{v} directly or fine-tune existing pretrained video generative models (Du et al., 2023; Liang et al., 2024; Hu et al., 2024; Liang et al., 2024; 2025; Pai et al., 2025). In cases where domain knowledge of the ground truth IDM is available, methods can leverage specialized pretrained models and algorithms to define \hat{h} . Examples include combining pretrained models for vision tasks (e.g., object tracking, optical flows) and inverse kinematics for robot manipulation (Ko et al., 2023; Liang et al., 2024). Additional considerations include interpretability (Liang et al., 2024), flexible goal specification through text-conditioning, and independence from a specific action space (Du et al., 2023; Ko et al., 2023). VM-IDM architectures have also been described as *Predictive Inverse Dynamics Models* (PIDM) and can also be trained end-to-end (Tian et al., 2024). Instead of sampling states from a VM, earlier work applies the IDM to a single action-free expert demonstration at inference time (Nair et al., 2017).

2.3.2. IDM LABELING

Another strategy is to train a policy $\hat{\pi}$ to predict the output of the trained IDM \hat{h} from (3). This is achieved by minimizing the cross-entropy loss $-\frac{1}{N} \sum_{i=1}^N \mathbb{E}_{\hat{h}(a|s_i, s'_i)} \log \hat{\pi}(a | s_i)$ w.r.t. $\hat{\pi}$ alone (\hat{h} is kept frozen), where all available pairs (s_i, s'_i) are used. This can also be understood as labeling the unlabeled transitions (s_i, s'_i) with actions sampled from the IDM, i.e. $\hat{a}_i \sim \hat{h}(a | s_i, s'_i)$, and finally training a policy via BC on the newly labeled transitions.

This simple 2-step formulation of IDM labeling was introduced and shown to work on Minecraft in VPT (Baker et al., 2022) using contractor data for \mathcal{D}_L and unlabeled online gameplay videos for \mathcal{D}_U . Variants of IDM labeling have been successfully applied to autonomous driving (Zhang et al., 2022), computer-use agents (Lu et al., 2025), and generated robot videos (Jang et al., 2025).

3. Connecting VM-IDM and IDM labeling

In this section, we show that, in the limit of infinitely many unlabeled pairs, VM-IDM and IDM labeling find the same policy, which we call the *IDM-based policy*. We then show that, when we have infinitely many labeled samples, the IDM-based policy recovers the expert π^* , just like BC.

We first note that the VM-IDM policy described in Section 2.3.1 can be written as

$$\hat{\pi}_{\hat{v}, \hat{h}}(a | s) := \int \hat{h}(a | s, s') \hat{v}(s' | s) ds', \quad (4)$$

where \hat{v} and \hat{h} are the learned VM and IDM, respectively.

To see this, observe that the sampling procedure from Section 2.3.1 corresponds to sampling from $\hat{h}(a | s, s') \hat{v}(s' | s)$ via *ancestral sampling* (Bishop, 2007, Section 8.1.2). Moreover, the integral marginalizing out s' reflects the fact that s' is discarded once the action is sampled.

Equivalence between VM-IDM and IDM labeling. In the VM-IDM method with infinitely many unlabeled pairs (s, s') , the VM learning objective stated in Section 2.3.1 becomes $-\mathbb{E}_{p_{\pi^*}(s)} \mathbb{E}_{p_{\pi^*}(s' | s)} \log \hat{v}(s' | s)$, which has the same minimizers as

$$\begin{aligned} & \mathbb{E}_{p_{\pi^*}(s)} \mathbb{E}_{p_{\pi^*}(s' | s)} [\log p_{\pi^*}(s' | s) - \log \hat{v}(s' | s)] \\ &= \mathbb{E}_{p_{\pi^*}(s)} D_{KL}(p_{\pi^*}(s' | s) \parallel \hat{v}(s' | s)). \end{aligned}$$

It is itself minimized precisely when $\hat{v}(s' | s)$ equals the ground-truth VM induced by the expert, defined by $v^*(s' | s) := p_{\pi^*}(s' | s)$. Note that $v^*(s' | s)$ can be derived from $p_{\pi^*}(s, a, s')$ using the definition of a conditional probability distribution/density. The policy obtained by combining this ground-truth VM v^* together with the learned IDM \hat{h} is thus $\hat{\pi}_{v^*, \hat{h}}$, reusing the notation from (4).

In IDM labeling with infinitely many unlabeled transitions, the learning objective from Section 2.3.2 becomes

$$-\mathbb{E}_{p_{\pi^*}(s) v^*(s' | s) \hat{h}(a | s, s')} \log \hat{\pi}(a | s),$$

which is equal to $-\mathbb{E}_{p_{\pi^*}(s) \hat{\pi}_{v^*, \hat{h}}(a | s)} \log \hat{\pi}(a | s)$. By a similar KL argument, it is minimized precisely when $\hat{\pi} = \hat{\pi}_{v^*, \hat{h}}$.

The last two paragraphs have showed that the policies learned by the VM-IDM approach and by IDM labeling are exactly the same and given by $\hat{\pi}_{v^*, \hat{h}}$ when (i) we have infinitely many unlabeled pairs (s, s') , (ii) the hypothesis class for \hat{v} and \hat{h} are expressive enough, and (iii) optimization finds a global minimizer. We refer to $\hat{\pi}_{v^*, \hat{h}}$ as the *IDM-based policy*.

Consistency of the IDM-based policy. We know that with infinitely many action-labeled samples (s, a, s') and sufficient capacity, the BC policy $\hat{\pi}_{BC}$ becomes equal to the expert policy π^* by the same KL argument used in the previous section. It is easy to see that this is also the case for the IDM-based policy. First, let us define the *ground-truth IDM induced by π^** as $h^*(a | s, s') := p_{\pi^*}(a | s, s')$, which can be derived from $p_{\pi^*}(s, a, s')$, defined in (1). With infinite labeled data and sufficient capacity, we can show via a routine KL argument that IDM learning recovers the ground-truth, i.e. $\hat{h} = h^*$. Consequently, $\hat{h}(a | s, s') v^*(s' | s) = p_{\pi^*}(a | s, s') p_{\pi^*}(s' | s) = p_{\pi^*}(a, s' | s)$. By integrating w.r.t. s' , we get $p_{\pi^*}(a | s) = \pi^*(a | s)$. In other words, the IDM-based policy learns the expert when given infinite action-labeled data. Note that we just showed $\hat{\pi}_{v^*, h^*} = \pi^*$.

Thus, BC, VM-IDM and IDM labeling are consistent procedures to estimate the expert policy π^* . However, we

will see that IDM-based policy learning can be much more label-efficient than BC.

4. Understanding IDM-based policies

Baker et al. (2022) argued that (i) IDM learning (Equation 3) is more sample efficient than BC and that (ii) this contributes to the superiority of IDM labeling policies against BC in SSIL. In this section, we begin by formalizing (i) and (ii), and then investigate specific explanations for (i).

The premise that “IDM learning is more sample efficient than BC” can be formalized as

$$\mathbb{E}_{p_{\pi^*}(s, s')} D_{KL}(h^* \parallel \hat{h}) < \mathbb{E}_{p_{\pi^*}(s)} D_{KL}(\pi^* \parallel \hat{\pi}_{BC}). \quad (5)$$

In other words, the learned IDM \hat{h} is closer to h^* than $\hat{\pi}_{BC}$ is to π^* , when both use the same amount of labeled data. Of course, if the learned IDM \hat{h} is close to h^* , we expect the IDM-based policies $\hat{\pi}_{v^*, \hat{h}}$ to be close to $\hat{\pi}_{v^*, h^*} = \pi^*$. We formalize this last point with the following inequality:

$$\mathbb{E}_{p_{\pi^*}(s)} D_{KL}(\pi^* \parallel \hat{\pi}_{v^*, \hat{h}}) \leq \mathbb{E}_{p_{\pi^*}(s, s')} D_{KL}(h^* \parallel \hat{h}), \quad (6)$$

proved in Appendix A. By combining (5) and (6), we obtain

$$\mathbb{E}_{p_{\pi^*}(s)} D_{KL}(\pi^* \parallel \hat{\pi}_{v^*, \hat{h}}) < \mathbb{E}_{p_{\pi^*}(s)} D_{KL}(\pi^* \parallel \hat{\pi}_{BC}),$$

suggesting IDM-based policies will outperform BC in SSIL.

In the rest of this section, we provide a more complete explanation of point (i), i.e. why IDM learning is more sample-efficient than BC. While the superior sample efficiency of IDM learning has been observed empirically in Minecraft (Baker et al., 2022) and in the context of VM-IDM policies for robotics (Liang et al., 2025; Pai et al., 2025), it is not entirely clear when and why this should be expected. Moreover, this point might be surprising given the IDM has *twice* as many inputs as the policy, implying a more complex hypothesis class typically leading to worst sample efficiency.

We attribute the superior sample efficiency of IDM learning against BC to two causes: First, the ground truth IDM h^* tends to be **less complex** (Section 4.1) and **less stochastic** (Section 4.2) than the expert π^* . Our analysis provides a more complete explanation for empirical observations and offers a valuable framework for understanding the performance gap between BC and IDM-based policies in different environments, as we will explore in Section 5.

4.1. Expert policy is more complex than IDM

In this section, we argue the following claim.

Claim 1. *The ground-truth IDM $h^*(a \mid s, s')$ is often less complex than the expert $\pi^*(a \mid s)$, and this contributes to IDM learning being more sample-efficient than BC.*

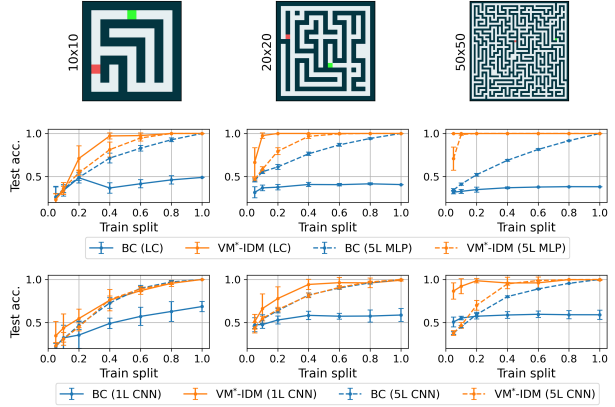


Figure 1. Varying the environment complexity. Comparing BC and VM-IDM, with different architectures for $\hat{\pi}$ and \hat{h} , respectively: *LC* is a linear classifier, *5L MLP* is a 5-layer multilayer perceptron and *nL CNN* is an n -layer convolutional neural network. See Appendix C.1 for details. Averaging over 5 seeds.

In other words, expressing π^* requires a more complex/expressive model than what is needed to express h^* which suggests that we can strike a better *bias-variance tradeoff* when learning h^* than when learning π^* . Indeed, if h^* is simple, it means there is a low complexity hypothesis class \mathcal{H} that contains h^* , which results in \hat{h} (Equation 3) being *unbiased*. Moreover, the fact that \mathcal{H} is low complexity means that \hat{h} has *low variance*. In contrast, since π^* is complex, it requires a larger hypothesis class Π to make sure $\hat{\pi}_{BC}$ (Equation 2) is unbiased, which in turn implies a larger variance and thus poorer generalization.

We investigate Claim 1 on simple maze environments generated and solved using `mazelab` (Zuo, 2018). We study two factors contributing to the complexity of π^* , namely *environment complexity* and *goal complexity*.

4.1.1. ENVIRONMENT COMPLEXITY

Experimental setup (Figure 1). We generate the transitions $(s, a, s') \in \mathcal{D}_L$ using the maze environment and an expert policy π^* solving the maze deterministically. We compare the test accuracy of BC and VM-IDM along four axes: *maze complexity*, *train split*, *state space format* & *model capacity*. *Maze complexity* refers to the size of the maze (10x10, 20x20 or 50x50). *Train split* refers to the proportion of states s that are present in the action-labeled dataset \mathcal{D}_L , where 1 means the full state space is sampled. The *state space format* is either \mathcal{S}^{pos} , where the state is the (x, y) coordinates of the agent, or \mathcal{S}^{img} , where the state is an image representation of the maze including the player and the goal. *Model capacity* takes two values, either *high* or *low*: When the state space format is \mathcal{S}^{pos} , \mathcal{H}_{low} and Π_{low} are linear classifiers (LC), while $\mathcal{H}_{\text{high}}$ and Π_{high} are multilayer perceptrons (MLP). When the state space format is \mathcal{S}^{img} , \mathcal{H}_{low} and Π_{low} are one-layer convolutional networks (1L CNN) and $\mathcal{H}_{\text{high}}$ and Π_{high}

are 5-layers CNNs (5L CNN). In all cases, the goal location is fixed across episodes (see Section 4.1.2 for experiments involving multiple goals). Note that, throughout Section 4.1, the VM-IDM uses the ground-truth video model v^* , echoing the infinite \mathcal{D}_U regime. For more details, see Appendix C.1.

Results (Figure 1). First, we see that for each maze environment and each state space format, the low capacity VM-IDM achieves perfect test accuracy when given enough samples (indicating $h^* \in \mathcal{H}_{\text{low}}$), while low-capacity BC policy never reaches perfect accuracy (indicating $\pi^* \notin \Pi_{\text{low}}$). This suggests that h^* is less complex than π^* . Secondly, while both low-capacity VM-IDM and high-capacity BC reach perfect performance when seeing enough data, the former outperforms the latter in the low data-regime; and this gap increases for more complex mazes. This suggests IDM learning is more sample-efficient than BC. Indeed, since h^* is simpler than π^* , we can use a smaller architecture to reduce variance without introducing bias, resulting in better test accuracy. Lastly, we observe that the high-capacity VM-IDM outperforms the high-capacity BC policy, especially for the more complex mazes. This trend is also present in the image state format, although not as strongly as for the position state format. We attribute this to the simplicity bias of neural networks which, while very expressive, have an implicit bias towards simpler functions. We will come back to this point soon.

Simple analytic form for h^* but not for π^* . We now show that the ground-truth IDM h^* can be expressed as a linear classifier, while the expert π^* cannot. In a maze, executing an action deterministically moves the agent in the corresponding direction by one unit unless a wall prevents this move. Since the expert policy π^* never runs into a wall, its induced ground-truth IDM h^* takes a particularly simple form. Indeed, this can be seen by noticing that, when avoiding walls, we can exactly infer the action taken from the state difference $s' - s$. For example, when $s' - s = (1, 0)^\top$, we can infer $a = \text{right}$; when $s' - s = (-1, 0)^\top$, we can infer $a = \text{left}$; and so on. Since the points $\{(1, 0), (-1, 0), (0, 1), (0, -1)\}$ are linearly separable and because the map $(s, s') \mapsto s' - s$ is linear, we can express $h^*(a \mid s, s')$ as $\text{softmax}_a(V(s, s'))$ for some matrix $V \in \mathbb{R}^{4 \times 4}$. We make this construction explicit in Appendix B.1. In other words, $h^* \in \mathcal{H}_{\text{low}}$, i.e. \hat{h} is unbiased. This explains why the low-capacity VM-IDM obtains perfect test accuracy in Figure 1 when trained on sufficiently many labeled samples. Now contrast this with the expert policy $\pi^*(a \mid s)$. For complex mazes, there is no obvious simple rule mapping the state s to the optimal action a . At the very least, it cannot be expressed by a linear classifier, as was the case for h^* . The expert π^* has to somehow “memorize” all the trajectories leading to the end of the maze. In this case, the expert policy π^* is much more complex than its corresponding ground-truth IDM h^* . The story is

similar when the state s is an image of the maze: We can formally show that the IDM h^* can be expressed with a simple single layer convolutional neural network (see Appendix B.2) while it appears the policy cannot (as suggested by its inferior performance in Figure 1).

Generalization via capacity control. Capacity control as a method to reduce variance is well-known: Reducing the size of the hypothesis class reduces the variance of the predictor. This common wisdom is formalized by the classical literature on statistical learning theory (Shalev-Shwartz & Ben-David, 2014; Mohri et al., 2018) which proposes quantitative measures of complexity for hypothesis classes which upperbound, with high probability, the difference between the generalization loss and the empirical loss of a learned predictor. Measures of complexity include the VC dimension (Vapnik & Chervonenkis, 1971) as well as the Rademacher complexity (Koltchinskii & Panchenko, 2000; Bartlett & Mendelson, 2003). These generalization bounds establish that controlling the capacity/expressivity of an hypothesis class reduces the variance of the learned predictor. This explains why the low-capacity VM-IDM policy (which we just showed is unbiased) outperforms the high-capacity one in the low-data regime.

Generalization via simplicity bias of NN. Note that capacity control cannot explain why, in Figure 1, the high-capacity VM-IDM policy outperforms the high-capacity BC policy in the low-data regime, since both \hat{h} and $\hat{\pi}_{\text{BC}}$ are implemented with the same 5-layer neural network. Even worse, we have in fact that the complexity of $\mathcal{H}_{\text{high}}$ is greater than that of Π_{high} , since the IDM has twice as many inputs as the policy, which suggests that $\hat{\pi}_{\text{BC}}$ should generalize better than $\hat{\pi}_{v^*, \hat{h}}$, contrary to our observation. We explain this observation by the *simplicity bias of neural networks*: When a neural network is in the *overparametrized interpolation regime*, i.e. when multiple parameter configurations achieve zero training loss, training tends to favor the interpolating functions which are simpler/smooth. We hypothesize that this simplicity bias favors the simpler h^* over the more complex π^* , thus explaining why fewer samples are needed to achieve greater performance for the VM-IDM policy. While the reasons why neural networks are implicitly biased towards simpler functions are not fully understood, theoretical explanations have been proposed, e.g. based on the regularizing effect of gradient-based optimization (Advani & Saxe, 2017; Soudry et al., 2018; Gidel et al., 2019) as well as based on the parameter-to-function map of neural architectures (Valle-Pérez et al., 2019; Mingard et al., 2021; Chiang et al., 2023; Buzaglo et al., 2024; Dziugaite & Roy, 2025).

4.1.2. GOAL COMPLEXITY

In the last section, we argued that the complexity of the environment impacts the complexity of the expert π^* with-

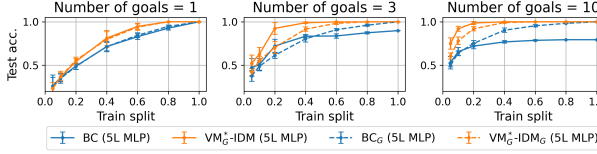


Figure 2. Varying the number of goals. BC_G is behavior cloning with goal conditioning, VM_G^{*}-IDM is VM^{*}-IDM where the VM is goal conditioned and the IDM is not; and VM_G^{*}-IDM_G is when both the VM and the IDM are goal conditioned. See Appendix C.1 for details. Averaging over 5 seeds.

out impacting that of the IDM h^* , leading to IDM learning having a statistical advantage over BC. We now argue that the *diversity of goals* also behaves in a similar way.

Experimental setup (Figure 2). We consider the same 10x10 maze environment as in Section 4.1.1, but this time the goal location changes from one trajectory to another. We assume the goal (x, y) -location, g , is observed with each transition (s, a, s') allowing *goal-conditioning* for each model. We compare the BC policy $\hat{\pi}_{\text{BC}}$ and the VM-IDM policy $\hat{\pi}_{v^*, \hat{h}}$ both with and without goal-conditioning, that is with and without g as input. For the VM-IDM policy, the video model is always goal-conditioned and equal to the ground-truth, i.e. $\hat{v}(s' | s, g) := p_{\pi^*}(s' | s, g)$. For the IDM, we have either $\hat{h}(a | s, s')$ or $\hat{h}(a | s, s', g)$.

Results (Figure 2). First, we see without surprise that BC without goal-conditioning cannot reach perfect test accuracy even when seeing all possible transitions (s, a, s') , i.e. it is biased. In contrast, VM-IDM without goal-conditioning does reach perfect test accuracy, indicating that the goal g is not necessary to predict the action given (s, s') , which of course makes intuitive sense in this simple environment. This is thus another way in which the IDM h^* is often less complex than the expert π^* , because the former effectively does not depend on g while the latter does. While BC with goal-conditioning does reach perfect accuracy with enough samples, in the low-data regime it is outperformed by VM-IDM, especially without goal-conditioning. This shows how IDM learning is more sample-efficient than BC.

4.2. Expert policy is more stochastic than IDM

In this section, we argue the following claim.

Claim 2. *The ground-truth IDM $h^*(a | s, s')$ is often less stochastic than the expert $\pi^*(a | s)$, and this contributes to IDM learning being more sample efficient than BC.*

In general, we always have $H(a | s, s') \leq H(a | s)$, where $H(a | s) := -\mathbb{E}_{s,a} \log \pi^*(a | s)$ and $H(a | s, s') := -\mathbb{E}_{s,a,s'} \log h^*(a | s, s')$ are *conditional entropies*. We claim that this inequality is often strict, meaning $h^*(a | s, s')$ is less stochastic on average than $\pi^*(a | s)$. This can happen, e.g., when multiple actions are equally optimal, al-

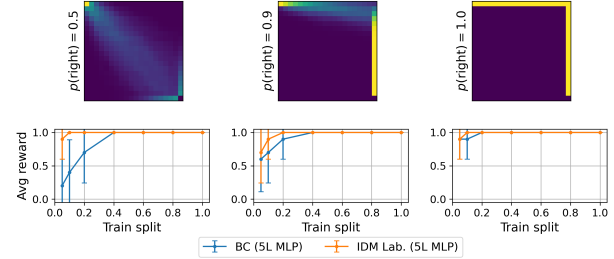


Figure 3. Varying the stochasticity of the expert. First row shows the state visitation distributions for different experts. Comparing the average reward of BC and IDM labeling. See Appendix C.1 for details. Averaging over 10 seeds.

lowing for a stochastic expert; and when observing (s, s') reveals with high certainty the action taken, which is the case in many navigation tasks (e.g. maze environments). This higher stochasticity makes BC less sample-efficient than IDM learning because the sample-efficiency of an estimator is often negatively impacted by the stochasticity of the ground-truth data-generating process (DGP). For example, in linear regression, the variance of the least-square estimator $\hat{\beta}$ is proportional to the variance of the residual noise ϵ in the DGP $y = \beta^* x + \epsilon$, under the Gauss-Markov conditions (Sen & Srivastava, 1991, Section 1.8). Also, generalization bounds for binary classification show how having a “likely not too stochastic” DGP $p^*(y | x)$ leads to improved sample efficiency (Mammen & Tsybakov, 1999).¹ We now investigate Claim 2 on a maze-like environment.

Experimental setup (Figure 3). We consider a simple 20x20 grid environment where the agent starts at the top left corner and must reach the bottom right corner. There are no obstacles preventing movement, except for the borders of the grid. We consider three expert policies to generate data. All three are optimal and consist in going right with probability $p(\text{right})$ and going down with probability $1 - p(\text{right})$, except when on a border, where the policy deterministically chooses the only optimal action. We vary $p(\text{right})$ to study the effect of the expert stochasticity on the performance of BC and IDM labeling. In both approaches, $\hat{\pi}$ and \hat{h} use the same MLP architecture. Note that the induced IDM h^* is always deterministic, contrary to π^* .

Results (Figure 3). In the low-data regime, we see that, as the stochasticity of the expert increases, the reward obtained by BC diminishes, contrarily to the IDM-based policy which is much less impacted. This is because the ground-truth IDM h^* remains deterministic, no matter how stochastic π^* is. This suggests the lower stochasticity of h^* contributes to its sample-efficiency.

¹We are referring to the Tsybakov noise condition (Mammen & Tsybakov, 1999). See Rigollet (2015, Section 3.2).

5. Methods and Experiments

The experiments of this section serve a dual purpose.

First, we aim to compare IDM-based policies, BC, and recent baselines for SSIL over a range of architectures and tasks, including Atari-like ProcGen environments with discrete actions (Section 5.1) and manipulation tasks with continuous actions (Section 5.2). When IDM-based policies outperform BC, we discuss if those gains can be plausibly attributed to the factors discussed in Section 4.

Second, we explore how the statistical advantage of IDM learning can be leveraged to improve other IDM-based SSIL methods. In particular, we propose an improved algorithm for latent action policy learning (Section 5.1) and show how sampling a model for unified video-action prediction as a VM-IDM improves policy success (Section 5.2).

5.1. ProcGen

LAPO. IDM-based methods typically train the IDM only on \mathcal{D}_L . Pretraining the IDM on \mathcal{D}_U has been the subject of recent research efforts leveraging *latent actions* (Edwards et al., 2019; Ye et al., 2022; Bruce et al., 2024; Ye et al., 2024). We specifically focus on the offline LAPO algorithm (Schmidt & Jiang, 2024), which we now describe.

In a **first stage**, LAPO pretrains jointly a *latent inverse dynamics model* (LIDM) $\tilde{h}(z | s, s')$ and a *latent forward dynamics model* (LFDM) $\tilde{f}(s' | s, z)$ to minimize the reconstruction loss $\frac{1}{N} \sum_{i=1}^N \|\hat{s}'_i - s'_i\|^2$ where $\hat{s}'_i \sim \tilde{f}(\cdot | s_i, z_i)$ and $z_i \sim \tilde{h}(\cdot | s_i, s'_i)$. The variable z is meant to be a continuous latent representation of the unobserved action. To induce an information bottleneck, LAPO additionally applies vector quantization to z before passing it to the LFDM (Bengio et al., 2013; Van Den Oord et al., 2017). In a **second stage**, a *latent action policy* $\tilde{\pi}(z | s)$ is trained to predict the output of the LIDM by minimizing $\frac{1}{N} \sum_{i=1}^N \|\hat{z}_i - z_i\|^2$ with $\hat{z}_i \sim \tilde{\pi}(\cdot | s_i)$, $z_i \sim \tilde{h}(\cdot | s_i, s'_i)$ and w.r.t. $\tilde{\pi}$ only, effectively implementing “latent IDM labeling”. We note that pre-quantized latent actions are used during this stage. The **third stage** decodes the output of $\tilde{\pi}$ to the true action space by minimizing $-\frac{1}{N} \sum_{i=1}^N \log \phi(a_i | z_i)$ w.r.t. to a decoding head ϕ only and using $z_i \sim \tilde{\pi}(\cdot | s_i)$. The composition $\phi \circ \tilde{\pi}$ forms the final policy $\hat{\pi}$.

LAPO+. We observe that the third stage of LAPO can be thought of as performing BC (Equation 2) on the labeled dataset \mathcal{D}_L with some fixed pretrained weights. We posit that decoding the LIDM instead—i.e. learning the IDM (Equation 3) with pretrained weights—will prove to be more sample-efficient (Section 4). Specifically, we use the same **first stage** as LAPO and consider a **second stage** where we decode the IDM $\hat{h} = \phi \circ \tilde{h}$ by minimizing $-\frac{1}{N} \sum_{i=1}^N \log \phi(a_i | z_i)$ w.r.t. to the decoding head ϕ only

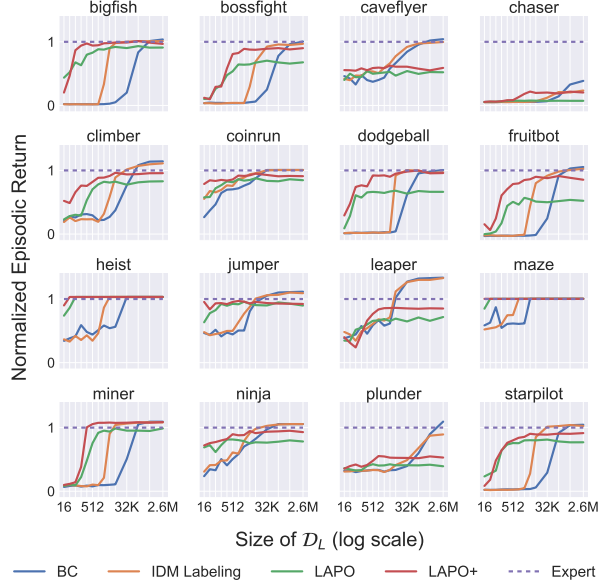


Figure 4. Normalized maximum return achieved during training by BC, IDM labeling, LAPO and LAPO+ in the 16 Atari-like ProcGen environments (Cobbe et al., 2019), varying the number of action-labeled transitions in \mathcal{D}_L . We show the average of 3 seeds, with \mathcal{D}_L being randomly sampled from the whole datasets each time. IDM labeling, LAPO and LAPO+ use all 2.6M transitions without action labels as \mathcal{D}_U .

and using $z_i \sim \tilde{h}(\cdot | s_i, s'_i)$. In the **third stage**, we learn the policy $\hat{\pi}$ by performing IDM labeling (Section 2.3.2) using labels generated from $\hat{h} = \phi \circ \tilde{h}$. We name this version of the algorithm **LAPO+**.

Results (Figures 4 & 5). We report the performance of BC, IDM labeling, LAPO and LAPO+ in ProcGen environments in Figure 4. Training details are provided in Appendix C.2.1. We find IDM labeling to outperform BC by a few orders of magnitude in 9 environments, while gains are modest or non-existent. In Figure 5, we discuss how the factors presented in Section 4 can shed light on the fluctuating sample efficiency gap between IDM labeling and BC.

For their part, LAPO & LAPO+ frequently yield capable policies vastly outperforming BC and IDM labeling in low-data regimes, with LAPO+ consistently outperforming LAPO. This underscores the importance of choosing the right latent function to decode with a small \mathcal{D}_L . Somewhat orthogonal to our claims, we note that LAPO and LAPO+ tend to underperform in high-data regimes, suggesting potential trade-offs associated with latent action policies.

5.2. Manipulation

Video-Action Multitasking. Recent methods for BC use unified, typically high-capacity architectures for video and action prediction where the VM and policy share most of

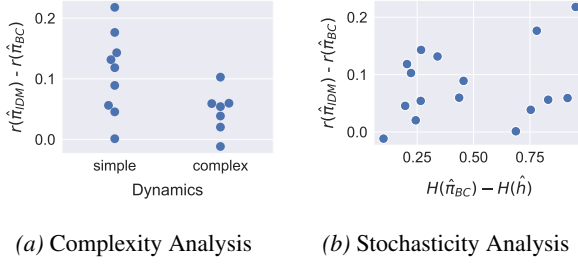


Figure 5. We study the complexity and stochasticity factors from Section 4 across the 16 ProcGen environments. As an aggregate score, we consider the mean return gap $r(\hat{\pi}_{IDM}) - r(\hat{\pi}_{BC})$ between IDM labeling and BC, which we average over \mathcal{D}_L sizes (Figure 4). **Complexity Analysis.** We divide environments based on their dynamics (Appendix C.2.2): *simple* environments are those the agent moves strictly because of an input action while the agent can move due to other factors in *complex* environments (e.g., momentum, gravity, moving platform). We expect the IDM to be simpler under simple dynamics and find the mean return gap to be higher in those environments. **Stochasticity Analysis.** As a proxy for the entropy of the ground truth policy and IDM in each environment, we consider the average conditional entropies on a test set of $\hat{\pi}_{BC}$ and the IDM \hat{h} learned on all 2.6M transitions, allowing us to study an approximate entropy gap $H(\hat{\pi}_{BC}) - H(\hat{h})$. We first note that $H(\hat{\pi}_{BC}) > H(\hat{h})$ across all environments, as hinted in Section 4.2. We then observe a positive, although imperfect correlation with the mean return gap.

their parameters (Wu et al., 2023; Guo et al., 2024). Follow-up works extend parameter sharing to IDMs and forward dynamics models (FDM), effectively learning a single model and relying on techniques such as input masking (Li et al., 2025) or separate diffusion timesteps (Zhu et al., 2025) to specifically sample the policy, the VM, the IDM or the FDM. We will refer to this setting as **multi-tasking**. Our experiments focus on UVA (Li et al., 2025), which has shown promising results on robot manipulation. We use the UVA architecture as a testbed to study BC and IDM-based policies using modern features such as diffusion action heads, frame stacking and action chunking. We emphasize that UVA uses a single architecture to implement the policy, VM, IDM and FDM.

Methods. We learn **BC**, **IDM labeling** and **VM-IDM** policies using the UVA architecture (without multitasking). We also train standard UVA (with multitasking) which samples actions from its policy (**Policy (UVA)**). As an alternative, we propose to sample actions as a VM-IDM (**VM-IDM (UVA)**). The latter is a compact parametrization of a VM-IDM and we hypothesize that it may lead to some improvements in the low-data regimes (Section 4). We follow the UVA recommendation to pretrain all models on the VM task on \mathcal{D}_U , meaning all models in this section perform SSIL via their initialization. Training details are provided in Appendix C.3.

Results (Figure 6). We compare these methods on Push-T and Libero10. IDM-based policies outperform BC in

most settings and by an especially large margin on Push-T, something we attribute to the particularly simple nature of the IDM on this problem (the action is the location of the agent). We note that IDM labeling tends to trail VM-IDM by a small margin. We speculate that this could be explained by the relatively limited size of \mathcal{D}_U (as opposed to the infinite regime considered in Section 3) and some generalization abilities of the VM. We finally observe that sampling the same UVA models as VM-IDMs leads to equal or improved performance over sampling them as policies, illustrating how UVA learns capable IDMs from relatively few samples.

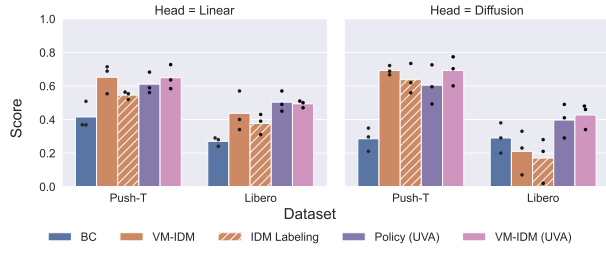


Figure 6. Policy performance on Push-T (Chi et al., 2025), which requires pushing a T-shaped block in a target position with a circular end-effector, and Libero10 (Liu et al., 2023), a set of 10 long-horizon robot manipulation tasks. For \mathcal{D}_L , we use 10 demonstrations for Push-T and 2 demonstrations per task for Libero10, representing approximately 5% of available demonstrations, which are all included without action labels in \mathcal{D}_U . The Push-T score is the average max IoU with the target T over 50 rollouts while the Libero10 score is the success rate over 100 rollouts. We report the performance of the last checkpoints averaged over 3 training seeds (we resample \mathcal{D}_L for each seed) and overlay the actual score of each seed as black markers. We also report results of a UVA variant with a linear action head.

6. Discussion

While the unifying concept of IDM-based policy (Section 3) and its formalism (Section 4) provide a valuable framework to understand the empirical performance of IDM-based policies in SSIL settings, some limitations remain. First, our modeling and experiments assume a curated \mathcal{D}_U which only includes expert data sampled precisely from the task of interest. A more practical setting would be when \mathcal{D}_U is sampled from an environment/expert that differs from the one of interest used to sample \mathcal{D}_L . Second, we focus on generalization and ignore sampling costs, with VM-IDM approaches being generally slower (although recent research efforts aim to address this shortcoming (Hu et al., 2024; Pai et al., 2025)). Finally, our work focuses on the sample efficiency of IDM learning w.r.t. action labels. We did not investigate the difference in generalization between VM-IDM and IDM labeling in the finite \mathcal{D}_U setting, which might be crucial to fully understand the differences between both methods. These present promising avenues for future work.

Acknowledgements

The work at the Université de Montréal was supported by a Natural Sciences and Engineering Research Council of Canada (NSERC) PGS D Scholarship (Morin). The authors would like to thank Simon Lacoste-Julien for engaging in insightful discussions that ultimately improved this work. This research was enabled in part by computational resources provided by Calcul Québec (calculquebec.ca), the Digital Research Alliance of Canada (alliancecan.ca) and Mila (mila.quebec).

Impact Statement

This paper presents work whose goal is to advance the field of Machine Learning. There are many potential societal consequences of our work, none which we feel must be specifically highlighted here.

References

Advani, M. and Saxe, A. High-dimensional dynamics of generalization error in neural networks. *Neural Networks*, 2017.

Baker, B., Akkaya, I., Zhokov, P., Huizinga, J., Tang, J., Ecoffet, A., Houghton, B., Sampedro, R., and Clune, J. Video pretraining (vpt): Learning to act by watching unlabeled online videos. *Advances in Neural Information Processing Systems*, 35:24639–24654, 2022.

Bartlett, P. L. and Mendelson, S. Rademacher and gaussian complexities: risk bounds and structural results. *J. Mach. Learn. Res.*, 2003.

Bengio, Y., Léonard, N., and Courville, A. Estimating or propagating gradients through stochastic neurons for conditional computation. *arXiv preprint arXiv:1308.3432*, 2013.

Bishop, C. M. *Pattern Recognition and Machine Learning (Information Science and Statistics)*. Springer, 2007.

Bruce, J., Dennis, M. D., Edwards, A., Parker-Holder, J., Shi, Y., Hughes, E., Lai, M., Mavalankar, A., Steigerwald, R., Apps, C., Aytar, Y., Bechtle, S. M. E., Behbahani, F., Chan, S. C., Heess, N., Gonzalez, L., Osindero, S., Ozair, S., Reed, S., Zhang, J., Zolna, K., Clune, J., de Freitas, N., Singh, S., and Rocktäschel, T. Genie: Generative interactive environments. In *Forty-first International Conference on Machine Learning*, 2024. URL <https://openreview.net/forum?id=bJbSbJskOS>.

Buzaglo, G., Harel, I., Nacson, M. S., Brutzkus, A., Srebro, N., and Soudry, D. How uniform random weights induce non-uniform bias: Typical interpolating neural networks generalize with narrow teachers. In *Proceedings of the 41st International Conference on Machine Learning*, 2024.

Chi, C., Xu, Z., Feng, S., Cousineau, E., Du, Y., Burchfiel, B., Tedrake, R., and Song, S. Diffusion policy: Visuomotor policy learning via action diffusion. *The International Journal of Robotics Research*, 44(10-11): 1684–1704, 2025.

Chiang, P., Ni, R., Miller, D. Y., Bansal, A., Geiping, J., Goldblum, M., and Goldstein, T. Loss landscapes are all you need: Neural network generalization can be explained without the implicit bias of gradient descent. In *The Eleventh International Conference on Learning Representations*, 2023.

Cobbe, K., Hesse, C., Hilton, J., and Schulman, J. Leveraging procedural generation to benchmark reinforcement learning. *arXiv preprint arXiv:1912.01588*, 2019.

Du, Y., Yang, S., Dai, B., Dai, H., Nachum, O., Tenenbaum, J., Schuurmans, D., and Abbeel, P. Learning universal policies via text-guided video generation. *Advances in neural information processing systems*, 36:9156–9172, 2023.

Dziugaite, G. K. and Roy, D. M. The size of teachers as a measure of data complexity: Pac-bayes excess risk bounds and scaling laws. In *Proceedings of The 28th International Conference on Artificial Intelligence and Statistics*, 2025.

Edwards, A., Sahni, H., Schroeder, Y., and Isbell, C. Imitating latent policies from observation. In *Proceedings of the 36th International Conference on Machine Learning*, pp. 1755–1763, 2019.

Espeholt, L., Soyer, H., Munos, R., Simonyan, K., Mnih, V., Ward, T., Doron, Y., Firoiu, V., Harley, T., Dunning, I., et al. Impala: Scalable distributed deep-rl with importance weighted actor-learner architectures. In *International conference on machine learning*, pp. 1407–1416. PMLR, 2018.

Gidel, G., Bach, F., and Lacoste-Julien, S. *Implicit regularization of discrete gradient dynamics in linear neural networks*. 2019.

Guo, Y., Hu, Y., Zhang, J., Wang, Y.-J., Chen, X., Lu, C., and Chen, J. Prediction with action: Visual policy learning via joint denoising process. *Advances in Neural Information Processing Systems*, 37:112386–112410, 2024.

Hu, Y., Guo, Y., Wang, P., Chen, X., Wang, Y.-J., Zhang, J., Sreenath, K., Lu, C., and Chen, J. Video prediction policy: A generalist robot policy with predictive visual representations. *arXiv preprint arXiv:2412.14803*, 2024.

Jang, J., Ye, S., Lin, Z., Xiang, J., Bjorck, J., Fang, Y., Hu, F., Huang, S., Kundalia, K., Lin, Y.-C., et al. Dreamgen: Unlocking generalization in robot learning through neural trajectories. *arXiv e-prints*, pp. arXiv–2505, 2025.

Ko, P.-C., Mao, J., Du, Y., Sun, S.-H., and Tenenbaum, J. B. Learning to act from actionless videos through dense correspondences. *arXiv preprint arXiv:2310.08576*, 2023.

Koltchinskii, V. and Panchenko, D. Rademacher processes and bounding the risk of function learning. In *High Dimensional Probability II*, 2000.

Li, S., Gao, Y., Sadigh, D., and Song, S. Unified video action model, 2025. URL <https://arxiv.org/abs/2503.00200>.

Li, T., Tian, Y., Li, H., Deng, M., and He, K. Autoregressive image generation without vector quantization. *Advances in Neural Information Processing Systems*, 37:56424–56445, 2024.

Liang, J., Liu, R., Ozguroglu, E., Sudhakar, S., Dave, A., Tokmakov, P., Song, S., and Vondrick, C. Dreamitate: Real-world visuomotor policy learning via video generation. *arXiv preprint arXiv:2406.16862*, 2024.

Liang, J., Tokmakov, P., Liu, R., Sudhakar, S., Shah, P., Ambrus, R., and Vondrick, C. Video generators are robot policies. *arXiv preprint arXiv:2508.00795*, 2025.

Liu, B., Zhu, Y., Gao, C., Feng, Y., Liu, Q., Zhu, Y., and Stone, P. Libero: Benchmarking knowledge transfer for lifelong robot learning. *Advances in Neural Information Processing Systems*, 36:44776–44791, 2023.

Lu, D., Xu, Y., Wang, J., Wu, H., Wang, X., Wang, Z., Yang, J., Su, H., Chen, J., Chen, J., et al. Videoagenttrek: Computer use pretraining from unlabeled videos. *arXiv preprint arXiv:2510.19488*, 2025.

Mammen, E. and Tsybakov, A. B. Smooth discrimination analysis. *The Annals of Statistics*, 1999.

Mingard, C., Valle-Pérez, G., Skalse, J., and Louis, A. A. Is sgd a bayesian sampler? well, almost. *Journal of Machine Learning Research*, 2021.

Mohri, M., Rostamizadeh, A., and Talwalkar, A. MIT Press, 2018.

Nair, A., Chen, D., Agrawal, P., Isola, P., Abbeel, P., Malik, J., and Levine, S. Combining self-supervised learning and imitation for vision-based rope manipulation. In *2017 IEEE international conference on robotics and automation (ICRA)*, pp. 2146–2153. IEEE, 2017.

O’Neill, A., Rehman, A., Maddukuri, A., Gupta, A., Padalkar, A., Lee, A., Pooley, A., Gupta, A., Mandlekar, A., Jain, A., et al. Open x-embodiment: Robotic learning datasets and rt-x models: Open x-embodiment collaboration 0. In *2024 IEEE International Conference on Robotics and Automation (ICRA)*, pp. 6892–6903. IEEE, 2024.

Pai, J., Achenbach, L., Montesinos, V., Forrai, B., Mees, O., and Nava, E. mimic-video: Video-action models for generalizable robot control beyond vlas. *arXiv preprint arXiv:2512.15692*, 2025.

Pomerleau, D. A. ALVINN: An autonomous land vehicle in a neural network. In *Advances in Neural Information Processing Systems*, 1988.

Radosavovic, I., Wang, X., Pinto, L., and Malik, J. State-only imitation learning for dexterous manipulation. In *2021 IEEE/RSJ International Conference on Intelligent Robots and Systems (IROS)*, pp. 7865–7871. IEEE, 2021.

Rigollet, P. Lecture notes. Mathematics of Machine Learning (18.657), MIT, 2015. URL https://ocw.mit.edu/courses/18-657-mathematics-of-machine-learning-fall-2015/81406c87dccb9e873cfafab76a4d69c3/MIT18_657F15_LecNote.pdf. Accessed: 2026-01-23.

Rombach, R., Blattmann, A., Lorenz, D., Esser, P., and Ommer, B. High-resolution image synthesis with latent diffusion models. In *Proceedings of the IEEE/CVF conference on computer vision and pattern recognition*, pp. 10684–10695, 2022.

Schmidt, D. and Jiang, M. Learning to act without actions. In *The Twelfth International Conference on Learning Representations*, 2024. URL <https://openreview.net/forum?id=rvUq3cxpDF>.

Sen, A. K. and Srivastava, M. S. Regression analysis: Theory, methods, and applications, 1991.

Shalev-Shwartz, S. and Ben-David, S. *Understanding Machine Learning: From Theory to Algorithms*. Cambridge University Press, 2014.

Soudry, D., Hoffer, E., Nacson, M. S., Gunasekar, S., and Srebro, N. The implicit bias of gradient descent on separable data. *Journal of Machine Learning Research*, 2018.

Sutton, R. S. and Barto, A. G. *Reinforcement Learning: An Introduction*. The MIT Press, 2018.

Tian, Y., Yang, S., Zeng, J., Wang, P., Lin, D., Dong, H., and Pang, J. Predictive inverse dynamics models are scalable learners for robotic manipulation. *arXiv preprint arXiv:2412.15109*, 2024.

Torabi, F., Warnell, G., and Stone, P. Behavioral cloning from observation. *arXiv preprint arXiv:1805.01954*, 2018.

Torabi, F., Warnell, G., and Stone, P. Recent advances in imitation learning from observation. *arXiv preprint arXiv:1905.13566*, 2019.

Valle-Pérez, G., Camargo, C. Q., and Louis, A. A. Deep learning generalizes because the parameter-function map is biased towards simple functions. *International Conference on Learning Representations*, 2019.

Van Den Oord, A., Vinyals, O., et al. Neural discrete representation learning. *Advances in neural information processing systems*, 30, 2017.

Vapnik, V. N. and Chervonenkis, A. Y. On the uniform convergence of relative frequencies of events to their probabilities. *Theory of Probability & Its Applications*, 1971.

Wu, H., Jing, Y., Cheang, C., Chen, G., Xu, J., Li, X., Liu, M., Li, H., and Kong, T. Unleashing large-scale video generative pre-training for visual robot manipulation. *arXiv preprint arXiv:2312.13139*, 2023.

Ye, S., Jang, J., Jeon, B., Joo, S., Yang, J., Peng, B., Mandlekar, A., Tan, R., Chao, Y.-W., Lin, B. Y., et al. Latent action pretraining from videos. *arXiv preprint arXiv:2410.11758*, 2024.

Ye, W., Zhang, Y., Abbeel, P., and Gao, Y. Become a proficient player with limited data through watching pure videos. In *The Eleventh International Conference on Learning Representations*, 2022.

Zhang, Q., Peng, Z., and Zhou, B. Learning to drive by watching youtube videos: Action-conditioned contrastive policy pretraining. In *European Conference on Computer Vision*, pp. 111–128. Springer, 2022.

Zhu, C., Yu, R., Feng, S., Burchfiel, B., Shah, P., and Gupta, A. Unified world models: Coupling video and action diffusion for pretraining on large robotic datasets. *arXiv preprint arXiv:2504.02792*, 2025.

Zuo, X. mazelab: A customizable framework to create maze and gridworld environments. <https://github.com/zuoxingdong/mazelab>, 2018.

A. Proof of Inequality 6

We now show that

$$\mathbb{E}_{p_{\pi^*}(s)} D_{KL}(\pi^*(a | s) \| \hat{\pi}_{v^*, \hat{h}}(a | s)) \leq \mathbb{E}_{p_{\pi^*}(s, s')} D_{KL}(h^*(a | s, s') \| \hat{h}(a | s, s'))$$

Proof

$$\begin{aligned} \mathbb{E}_{p_{\pi^*}(s, s')} D_{KL}(h^*(a | s, s') \| \hat{h}(a | s, s')) &= \mathbb{E}_{p_{\pi^*}(s, s')} \sum_{a \in \mathcal{A}} h^*(a | s, s') \log \frac{h^*(a | s, s')}{\hat{h}(a | s, s')} \\ &= \mathbb{E}_{p_{\pi^*}(s)} \int \sum_{a \in \mathcal{A}} v^*(s' | s) h^*(a | s, s') \log \frac{h^*(a | s, s')}{\hat{h}(a | s, s')} ds' \\ &= \mathbb{E}_{p_{\pi^*}(s)} \int \sum_{a \in \mathcal{A}} v^*(s' | s) h^*(a | s, s') \log \frac{h^*(a | s, s') v^*(s' | s)}{\hat{h}(a | s, s') v^*(s' | s)} ds' \\ &= \mathbb{E}_{p_{\pi^*}(s)} \int \sum_{a \in \mathcal{A}} p_{\pi^*}(a, s' | s) \log \frac{p_{\pi^*}(a, s' | s)}{\hat{h}(a | s, s') v^*(s' | s)} ds'. \end{aligned}$$

Define $p_{v^*, \hat{h}}(a, s' | s) := \hat{h}(a | s, s') v^*(s' | s)$. From this we obtain

$$\begin{aligned} \mathbb{E}_{p_{\pi^*}(s, s')} D_{KL}(h^*(a | s, s') \| \hat{h}(a | s, s')) &= \mathbb{E}_{p_{\pi^*}(s)} \int \sum_{a \in \mathcal{A}} p_{\pi^*}(a, s' | s) \log \frac{p_{\pi^*}(a, s' | s)}{p_{v^*, \hat{h}}(a, s' | s)} ds' \\ &= \mathbb{E}_{p_{\pi^*}(s)} D_{KL}(p_{\pi^*}(a, s' | s) \| p_{v^*, \hat{h}}(a, s' | s)) \\ &= \mathbb{E}_{p_{\pi^*}(s)} D_{KL}(p_{\pi^*}(a | s) \| p_{v^*, \hat{h}}(a | s)) + \mathbb{E}_{p_{\pi^*}(s, a)} D_{KL}(p_{\pi^*}(s' | s, a) \| p_{v^*, \hat{h}}(s' | s, a)) \\ &= \mathbb{E}_{p_{\pi^*}(s)} D_{KL}(\pi^*(a | s) \| \hat{\pi}_{v^*, \hat{h}}(a | s)) + \mathbb{E}_{p_{\pi^*}(s, a)} D_{KL}(p(s' | s, a) \| p_{v^*, \hat{h}}(s' | s, a)) \\ &\geq \mathbb{E}_{p_{\pi^*}(s)} D_{KL}(\pi^*(a | s) \| \hat{\pi}_{v^*, \hat{h}}(a | s)), \end{aligned}$$

where we leveraged the chain rule for the KL divergence in the third equality and the fact that the KL divergence is always greater or equal to zero in the last inequality. \blacksquare

B. Explicit expressions for simple ground-truth IDM in Figure 1

B.1. Positions as states (\mathcal{S}_{pos})

We now show that the ground-truth IDM h^* from Figure 1 with position states (\mathcal{S}_{pos}) can be expressed as a linear classifier. Executing an action deterministically moves the player in the corresponding direction by one unit unless a wall prevents this move. Assuming the expert policy π^* never runs into a wall (which is the case here), its induced ground-truth IDM h^* takes a particularly simple form. Indeed, this can be seen by noticing that, when avoiding walls, we can exactly infer the action taken from the state difference $s' - s$. For example, when $s' - s = (1, 0)^\top$, we can infer $a = \text{right}$; when $s' - s = (-1, 0)^\top$, we can infer $a = \text{left}$; and so on. Moreover, the map from $s' - s$ to a can be expressed with a simple linear classifier $\text{softmax}_a(\tau^{-1}W(s' - s))$ where τ is a temperature parameter and

$$W := \begin{bmatrix} 1 & -1 & 0 & 0 \\ 0 & 0 & 1 & -1 \end{bmatrix}^\top.$$

Importantly, when $\tau \rightarrow 0$, we have that $\text{softmax}_a(\tau^{-1}W(s' - s))$ approaches the ground-truth IDM $h^*(a | s, s')$, since it concentrates probability mass on the correct action. Since the map $(s, s') \mapsto \tau^{-1}W(s' - s)$ is linear, we have that h^* can be (approximately) expressed by a linear classifier. In other words, h^* is in the closure of \mathcal{H}_{low} .

B.2. Images as states (\mathcal{S}_{img})

We now show that the ground-truth IDM h^* from Figure 1 with image states (\mathcal{S}_{img}) can be expressed as a simple one-layer network with a convolutional layer with a 3x3 kernel, mapping the 6 input channels (s and s' have three channels each) to 4 channels (one per action) without padding nor stride; with a global max pooling layer (same as described in C.1.1). For each action a , we construct the 3x3 kernel $K^a \in \mathbb{R}^{6 \times 3 \times 3}$. Let $x, x' \in \mathbb{R}^{3 \times 3 \times 3}$ be a 3x3 patch of s and s' (taken at the same location). We can see K^a as the concatenation of two kernels, namely $W^a, V^a \in \mathbb{R}^{3 \times 3 \times 3}$. The dot product between the kernel $K^a = (W^a, V^a)$ and the patch (x, x') can thus be written as

$$\langle K^a, (x, x') \rangle = \langle W^a, x \rangle + \langle V^a, x' \rangle$$

By setting $W^a := -V^a$ we get

$$\langle K^a, (x, x') \rangle = \langle -V^a, x \rangle + \langle V^a, x' \rangle = \langle V^a, -x \rangle + \langle V^a, x' \rangle = \langle V^a, x' - x \rangle.$$

Interestingly, $x' - x$ acts as a motion detector. Meaning, if nothing changes between x and x' , it means (i) the agent does not appear in x nor x' , or (ii) the agent appears in both but did not move. Since π^* leads to an agent that allows move, since it never runs into walls, $x - x' = 0$ must imply the agent does not appear in x nor x' . Let $(x_{\text{right}}, x'_{\text{right}})$ be a pair of patches corresponding to the same image location where the agent is located at the center of the patch x_{right} and move one step to the right in patch x'_{right} . We can define the pairs $(x_{\text{left}}, x'_{\text{left}})$, $(x_{\text{up}}, x'_{\text{up}})$ and $(x_{\text{down}}, x'_{\text{down}})$ analogously. Then, we can define V^a as

$$V^{\text{right}} := x'_{\text{right}} - x_{\text{right}}, \quad V^{\text{left}} := x'_{\text{left}} - x_{\text{left}}, \quad V^{\text{up}} := x'_{\text{up}} - x_{\text{up}}, \quad V^{\text{down}} := x'_{\text{down}} - x_{\text{down}}.$$

From this, it is clear that $\langle K^{\text{right}}, (x, x') \rangle$ will be maximized precisely when the patch (x, x') is such that the agent is centered in x and moved to the right in x' ; and analogously for the other actions. We can define the score (pre-softmax) as

$$z^a(s, s') := \max_{i,j} \langle K^a, (x_{i,j}, x'_{i,j}) \rangle \text{ for all } a,$$

where $(x_{i,j}, x'_{i,j})$ corresponds to the 3x3 patch at location i, j in (s, s') . We can collect these scores into a vector $z(s, s') := (z^a(s, s'))_{a \in \mathcal{A}}$ and pass it into a softmax to get $\hat{h}(a | s, s') := \text{softmax}_a(\tau^{-1}z(s, s'))$ where τ is a temperature parameter.

We now show that, for any feasible transition (s, a^*, s') , we have $a^* = \arg \max_a z^a(s, s')$ and this maximizer is unique. If that is the case, we can easily see that $\hat{h}(a | s, s') \rightarrow \mathbf{1}(a = a^*) = h^*(a | s, s')$ as $\tau \rightarrow 0$ (showing that the ground-truth IDM can be expressed with this 1L CNN).

Fix some transition (s, a^*, s') . It is clear that there will be a location (i^*, j^*) such that the agent is at the center of the 3x3 patch x_{i^*, j^*} of s . Since the agent moved in direction a^* , we have

$$\begin{aligned} z^{a^*}(s, s') &= \max_{i,j} \langle K^{a^*}, (x_{i,j}, x'_{i,j}) \rangle = \langle K^{a^*}, (x_{i^*, j^*}, x'_{i^*, j^*}) \rangle = \langle V^{a^*}, x'_{i^*, j^*} - x_{i^*, j^*} \rangle = \langle x'_{a^*} - x_{a^*}, x'_{i^*, j^*} - x_{i^*, j^*} \rangle \\ &= \|x'_{a^*} - x_{a^*}\|_2^2 \end{aligned}$$

Moreover, no other action $a \neq a^*$ and grid location (i, j) will give a score $\langle K^a, (x_{i,j}, x'_{i,j}) \rangle = \langle V^a, x'_{i,j} - x_{i,j} \rangle$ larger or equal to $\|x'_{a^*} - x_{a^*}\|_2^2$. This means a^* is the unique maximizer of $z^a(s, s')$.

C. Experiments

C.1. Maze/grid Experiments

C.1.1. ARCHITECTURES

LC - Linear Classifier (Figure 1, with \mathcal{S}_{pos}). It corresponds to $\hat{\pi}(a | s) = \text{softmax}_a(Ws + b)$ where $W \in \mathbb{R}^{4 \times 2}$ and $b \in \mathbb{R}^4$ and $\hat{h}(a | s, s') = \text{softmax}_a(V(s, s') + c)$ where $V \in \mathbb{R}^{4 \times 4}$ and $b \in \mathbb{R}^4$.

5L MLP - Multilayer Perceptron (Figures 1, 2 & 3, with \mathcal{S}_{pos}). It consists of a multilayer neural network with 5 hidden layers of 100 neurons with ReLU nonlinearities. The output is a softmax over the four possible actions. The input dimension

depends on the setting: 2 inputs when used as a policy and 4 inputs when used as an IDM. In both cases, we add 2 input dimensions when goal conditioning (the goal is an (x, y) -location).

1L CNN - One-layer convolutional neural network with global max pooling (Figure 1, with \mathcal{S}_{img}). It has one convolutional layer with a 3x3 kernel, mapping the input channels (3 input channels for $\hat{\pi}(a | s)$ and 6 input channels for $\hat{h}(a | s, s')$) to 4 channels (one per action) without padding nor stride. Next, the maximum is taken across pixels (reducing the width and height dimensions), which results in a 4-dimensional vector which is then fed into a softmax function to obtain a distribution over actions.

5L CNN - 5-layer convolutional neural network (Figure 1, with \mathcal{S}_{img}). The number of input channels is 3 for $\hat{\pi}(a | s)$ and 6 for $\hat{h}(a | s, s')$. Three blocks of the form ‘‘convolution-ReLU-MaxPool’’ are applied, where the convolution has a 3x3 kernel with 128 output channels (padding=1, no stride) and the MaxPool layer has a 2x2 kernel (no padding, no stride). Then, two fully connected ReLU layers are applied, with 128 hidden units each. A final linear projection maps to a 4-dimensional vector, which is fed to a softmax to obtain a distribution over actions.

C.1.2. COMPLEXITY EXPERIMENTS (FIGURES 1 & 2) – ENVIRONMENTS, DATASETS & METRICS

The three mazes were randomly generated and solved using the `mazelab` library (Zuo, 2018). The action space is $\mathcal{A} := \{\text{right}, \text{left}, \text{up}, \text{down}\}$ and executing one of these deterministically moves the player in the corresponding direction (by one unit) unless a wall prevents this move, in which case the player remains static. Note that the resulting expert π^* is always deterministic, allowing us to write $\pi^*(s)$ to denote the action taken by π^* in state s . Moreover, the environment dynamics is also deterministic, i.e. $p(s' | s, a) = \mathbf{1}(s' = f(s, a))$ for some function f where $\mathbf{1}(\cdot)$ is the indicator function, which means the ground-truth video model v^* induced by the expert is also deterministic. Indeed,

$$v^*(s' | s) = \sum_a p(s' | s, a) \pi^*(a | s) = \sum_a \mathbf{1}(s' = f(s, a)) \mathbf{1}(a = \pi^*(s)) = \mathbf{1}(s' = f(s, \pi^*(s))).$$

Define $v^*(s) := f(s, \pi^*(s))$.

With this notation setup, we have that the test set is given by

$$\mathcal{D}_L^{\text{test}} := \{(s, \pi^*(s), v^*(s)) \mid s \in \mathcal{S}_{\text{feasible}}\},$$

where $\mathcal{S}_{\text{feasible}}$ is the set of feasible states. The training set $\mathcal{D}_L^{\text{train}}$ is constructed by randomly sampling a fraction of the test set without replacement. In the goal conditioning experiment of Figure 2, the goal description g is added as a feature.

The **test accuracy** of a learned policy $\hat{\pi}$ is given by

$$\text{Acc}_{\text{test}}(\hat{\pi}) := \frac{1}{|\mathcal{D}_L^{\text{test}}|} \sum_{(s, a, s') \in \mathcal{D}_L^{\text{test}}} \mathbf{1}(a = \hat{\pi}(s)),$$

where $\hat{\pi}(s) := \arg \max_a \hat{\pi}(a | s)$.

Remark C.1. In this deterministic setup, the IDM-based policy $\hat{\pi}_{v^*, \hat{h}}$ (Section 3) takes the particularly simple form $\hat{\pi}_{v^*, \hat{h}}(a | s) = \hat{h}(a | s, v^*(s))$. Indeed,

$$\hat{\pi}_{v^*, \hat{h}}(a | s) = \sum_{s'} \hat{h}(a | s, s') v^*(s' | s) = \sum_{s'} \hat{h}(a | s, s') \mathbf{1}(s' = v^*(s)) = \hat{h}(a | s, v^*(s)).$$

Remark C.2. The test accuracy of the IDM \hat{h} is the same as the accuracy of the IDM-based policy $\hat{\pi}_{v^*, \hat{h}}$. Indeed, by defining $\hat{h}(s, s') = \arg \max_a \hat{h}(a | s, s')$, we get

$$\begin{aligned} \text{Acc}_{\text{test}}(\hat{h}) &:= \frac{1}{|\mathcal{D}_L^{\text{test}}|} \sum_{(s, a, s') \in \mathcal{D}_L^{\text{test}}} \mathbf{1}(a = \hat{h}(s, s')) \\ &= \frac{1}{|\mathcal{D}_L^{\text{test}}|} \sum_{(s, a, s') \in \mathcal{D}_L^{\text{test}}} \mathbf{1}(a = \hat{h}(s, v^*(s))) \\ &= \frac{1}{|\mathcal{D}_L^{\text{test}}|} \sum_{(s, a, s') \in \mathcal{D}_L^{\text{test}}} \mathbf{1}(a = \hat{\pi}_{v^*, \hat{h}}(s)) = \text{Acc}_{\text{test}}(\hat{\pi}_{v^*, \hat{h}}). \end{aligned}$$

Remark C.3. The definition and claims made above remain identical with goal conditioning, simply replace s by (s, g) .

C.1.3. STOCHASTICITY EXPERIMENT (FIGURE 3): ENVIRONMENTS, DATASETS & METRICS

As explained in Section 4.2, we consider a simple 20x20 grid environment where the agent starts at the top left corner and must reach the bottom right corner. The action space is again $\mathcal{A} := \{\text{right}, \text{left}, \text{up}, \text{down}\}$. There are no obstacles preventing movement, except for the borders of the grid. We consider three expert policies used to generate the training data. All three are optimal and consist in going right with probability $p(\text{right})$ and going down with probability $1 - p(\text{right})$, except when on the right or bottom border, where the policy deterministically chooses the only optimal action. We vary $p(\text{right})$ to study the effect of the stochasticity of the expert on the performance of BC and IDM labeling.

For each expert, we sample 26 full trajectories of length 38 (this is the number of actions required to solve the environment) for a total of 988 transitions (s, a, s') . These transitions form the dataset $\mathcal{D}^{\text{full}}$. The unlabeled dataset \mathcal{D}_U is obtained by discarding the action labels in $\mathcal{D}^{\text{full}}$. The action-labeled training set \mathcal{D}_L is formed by sampling a fraction of $\mathcal{D}_L^{\text{full}}$ without replacement (“train split” corresponds to that fraction). Note that the IDM \hat{h} is trained on \mathcal{D}_L while $\hat{\pi}$ is trained on \mathcal{D}_U via the IDM labeling objective from Section 2.3.2.

The **average reward** measures the performance of a policy $\hat{\pi}$ by averaging the reward obtained over 25 episodes, each limited to 38 steps (the minimum necessary to reach the end goal). A reward of one is obtained if the goal is reached within 38 steps, otherwise the reward is 0.

Remark C.4. Note that accuracy is not a good metric to measure the performance of a policy $\hat{\pi}$ when the expert π^* is stochastic. This is why we instead report the average reward.

C.1.4. OPTIMIZATION

In all maze/grid experiments (Figures 1, 2 & 3), we train using the Adam optimizer. To train LC and 5L MLP, we use a learning rate of 1e-3, while we use 1e-4 for 1L CNN and 5L CNN. For the CNN architecture we use a batch size of $\min\{32, |\mathcal{D}_L|\}$ while we use a batch size of $|\mathcal{D}_L|$ for the MLP experiments, except for the policies of Figure 3, where we used a batch size of $\min\{512, |\mathcal{D}_L|\}$ for BC and $\min\{512, |\mathcal{D}_U|\}$ for IDM Labeling.

C.2. ProcGen Experiments

C.2.1. TRAINING DETAILS

In ProcGen environments, s and s' are RGB frames and a is a discrete action. We use the data and learning setup from LAPO (Schmidt & Jiang, 2024), relying on IMPALA-CNNs (Espeholt et al., 2018) followed by a fully-connected action decoder with hidden sizes (128, 128) to implement BC, IDM labeling, LAPO and LAPO+. We still train the action decoder (end-to-end with the backbone) during BC and IDM labeling for parity. We use a learning rate of 2e-4 (except for LAPO/LAPO+ stage 1 where we use 3e-4), a piecewise linear schedule, a batch size of $\min\{128, |\mathcal{D}_L|\}$ (or 128 if only \mathcal{D}_U is used) and the Adam optimizer. To ensure a fair comparison, we make sure the total number of training steps across all stages sums to 120,000 for all methods. Specifically, we use 120,000 steps for BC, 60,000/60,000 steps for the two stages of IDM labeling, 50,000/60,000/10,000 steps for the three LAPO stages, and 50,000/10,000/60,000 steps for the three LAPO+ stages.

For latent action policies, we do not retrain LAPO stage 1 for each seed and instead use the same stage 1 models (one for each environment) for all downstream LAPO and LAPO+ runs. We reuse the quantization hyperparameters from (Schmidt & Jiang, 2024) for LAPO stage 1. While LAPO originally included one additional frame of pre-transition context for the LIDM, we do not include any pre-transition context to simplify the comparison between IDM-based methods and BC.

C.2.2. COMPLEXITY CLASSIFICATION

We consider the `bigfish`, `bossfight`, `dodgeball`, `fruitbot`, `heist`, `maze`, `miner`, `plunder` and `starpilot` environments as having simple dynamics. We consider the following environments as complex: `caveflyer` and `chaser` because of momentum (agent does not stop immediately given no inputs), `climber`, `coinrun`, `jumper` and `ninja` because of gravity, and `leaper` because of moving platforms.

C.3. Manipulation Experiments

For Push-T and Libero10, s and s' include four RGB frames each and a is a block of 16 continuous action vectors. We use the UVA codebase (Li et al., 2025). UVA is initialized with the pretrained image generation model MAR-B (Li et al.,

2024) and encodes all images using a frozen VAE KL-16 (Rombach et al., 2022). The architecture relies on a transformer backbone and two separate diffusion heads for video generation and action generation. We refer to the original paper for details. The UVA architecture implements the following task modes through input masking and selective output decoding: policy, VM, FDM, IDM and a *full dynamics model* (i.e., $p(a, s'|s)$). We modified the UVA masking procedure to include all current frames s in the IDM to put it on par with the policy. For a given batch during training, UVA uniformly samples a task, applies masking to the irrelevant inputs, and computes the loss for the sampled task. We use a learning rate of 2e-5, a batch size of 128, and train all models for 50,000 steps using the AdamW optimizer on nodes with 4xH100 GPUs.

We pretrain UVA in VM mode only on \mathcal{D}_U for each environment and use this as an initialization for all methods, per the UVA training recommendations. As such, all methods in this section perform SSIL via their initialization. We then disable the other task modes to learn single functions and perform BC or IDM learning on \mathcal{D}_L . Next, we use the same IDMs for IDM labeling (again starting from the VM initialization and fitting UVA in policy mode on the IDM-labeled \mathcal{D}_U) or VM-IDM (pairing the IDMs with the initial VM). We also train standard UVA with multitasking on \mathcal{D}_L and show the performance of the two sampling paths Policy (UVA) and Video-IDM (UVA).

We experienced relatively high variance when training with diffusion heads on Libero10 (perhaps due to the limited size of \mathcal{D}_L) and chose to include results of a UVA variant with a linear action head due to its overall stronger performance on this benchmark. We use a SmoothL1 loss with $\beta = 1.0$ in this case.